We are IntechOpen, the world's leading publisher of Open Access books Built by scientists, for scientists

4,800
Open access books available

122,000
International authors and editors

135M
Downloads

Our authors are among the

154
Countries delivered to

TOP 1%
most cited scientists

12.2%
Contributors from top 500 universities

WEB OF SCIENCE™

Selection of our books indexed in the Book Citation Index in Web of Science™ Core Collection (BKCI)

Interested in publishing with us?
Contact book.department@intechopen.com

Numbers displayed above are based on latest data collected.
For more information visit www.intechopen.com

2

Susceptibility of Epithelium to PTEN-Deficient Tumorigenesis

Chun-Ming Chen[1,2], Tsai-Ling Lu[1], Fang-Yi Su[1] and Li-Ru You[2, 3]
[1]*Department of Life Sciences and Institute of Genome Sciences,*
[2]*VGH-YM Genome Center,*
[3]*Institute of Biochemistry and Molecular Biology,*
National Yang-Ming University, Taipei,
Taiwan

1. Introduction

Phosphatase and tension homolog deleted on chromosome 10, *PTEN*, is a tumor suppressor gene that is responsible for controlling tumorigenesis in various organs (Li and Sun 1997, Steck et al. 1997, Li et al. 1997, Ali, Schriml and Dean 1999). Functionally, PTEN exhibits phospholipid phosphatase activity and negatively regulates the conversion of phosphatidylinositol 4, 5-diphosphate (PIP2) to PIP3 (Stambolic et al. 1998, Wu et al. 1998). PTEN ablation results in the accumulation of PIP3, which recruits AKT to the cell membrane, where PIP3-dependent protein kinase-1 (PDK1) and mammalian target of rapamycin (mTOR) complex 2 (mTORC2), also known as the Rictor-mTOR complex, activate and phosphorylate AKT at amino acid residues Thr308 and Ser473, respectively (Alessi et al. 1997, Sarbassov et al. 2004, Sarbassov et al. 2005). Consequently, activated AKT acts as a key effector and modulates a variety of downstream signal regulators. One AKT-targeting protein is tuberous sclerosis complex 2 (TSC2) (Inoki et al. 2002, Manning et al. 2002), which is a GTPase-activating protein that forms a complex with TSC1 to block a small GTPase Rheb at GDP-bound status, consequently resulting in mTORC1 (the Raptor-mTOR complex) inhibition. Thus, AKT-mediated TSC1-TSC2 inhibition results in mTORC1 activation, which promotes cell growth and protein translation partly through phosphorylating S6 kinase (S6K) and the eIF-4E-binding protein 1 (4E-BP1) (Brunn et al. 1997, Hara et al. 1997, Brown et al. 1995). Activated mTORC1 and S6K can also regulate PI3K-AKT signaling through a negative feedback mechanism [see Fig 1; reviewed in (Carracedo and Pandolfi 2008, Manning and Cantley 2007)]. In addition, activated AKT can target glycogen synthase kinase 3 (GSK3) (Cross et al. 1995), β-catenin (Fang et al. 2007, He et al. 2007), double minute 2 (Mdm2) (Mayo and Donner 2001, Zhou et al. 2001b), p21 (Zhou et al. 2001a), p27 (Fujita et al. 2002), forkhead-related transcription factors (Brunet et al. 1999), Bcl2-antagonist of cell death (Datta et al. 1997, Peso et al. 1997), and other genes, leading to cellular proliferation, anti-apoptosis, survival, and tumorigenesis [see Fig 1; (Cully et al. 2006, Kishimoto et al. 2003, Manning and Cantley 2007, Dunlop and Tee 2009)].
To model *Pten*-deficient malignancies, conditional *Pten* mutant alleles have been generated in mice. Using tissue-specific Cre-*lox*P-mediated *Pten* gene excision, the roles of *Pten* have been intensively studied across multiple organs in mice. We previously used an inducible

Cre under the control of a ubiquitous promoter, *ROSA26* (*R26*), to examine the susceptibility of all tissues to *Pten*-deficient tumorigenesis in an adult mice strain referred to as *R26-Pten*$^{fx/fx}$. We found that lymphomas accounted for the majority of *Pten*-deficient malignancies (Lu et al. 2007). However, the high incidence and short latency of lymphomas in the *R26-Pten*$^{fx/fx}$ mice limited our analyses of the tumors arising from the epithelial tissues, the most common origin of human cancers. To address the susceptibility of epithelial tissues to *Pten* loss, we performed spatiotemporally controlled *Pten* excision by using a newly generated inducible Cre transgene driven by the keratin 8 (K8) promoter in a mouse strain referred to as *K8-Pten*$^{fx/fx}$. In this epithelial *Pten*-deficient mouse, multiple epithelial tumors arose, and they could be monitored at different time points after *Pten* was ablated.

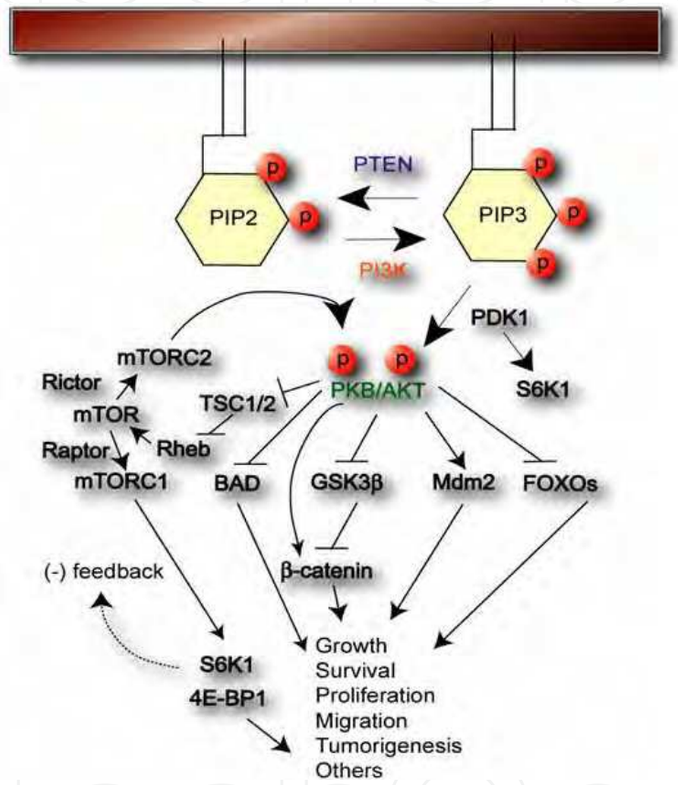

Fig. 1. Schematic illustration of PTEN/PI3K/AKT and their downstream effectors.

2. Genetic tool for conditional genetic manipulation in the epithelial tissues

To develop transgenic mice expressing inducible Cre (CreER^T) in epithelial tissues, we generated and characterized the transgenic mouse line *Tg(K18-EGFP, K8-CreER^T)*, in which the visualized enhanced green fluorescence protein (EGFP) is driven by the K18 upstream regulatory elements and the *CreER^T* fusion gene is driven by *K8* (Fig 2). To evaluate the induced *CreER^T* recombinase activity after tamoxifen (Tam) administration, *Tg(K18-EGFP,K8-CreER^T)* mice, hereafter abbreviated as *K18-EG/K8-CE*, were bred with *ROSA26 Cre* reporter (*R26R*$^{LacZ/+}$) mice (Soriano 1999) to generate *K18-EG/K8-CE*$^{tg/+}$*;R26R*$^{LacZ/+}$ bigenic mice.

We monitored K18 promoter-directed EGFP expression in the offspring of C57BL/6 females, which were bred with different lines of *K18-EG/K8-CE* males. We found that lines B, G, and H among eight transgenic lines exhibited strong and consistent EGFP signals in the tail,

footpads, and all internal organs lined by simple epithelium (data not shown). Subsequently, these three lines were selected to breed with *R26R*$^{LacZ/+}$ mice to generate double-transgenic mice (referred to *K18-EG/K8CE*$^{tg/+}$*;R26R*$^{LacZ/+}$), which were evaluated by whole mount X-gal staining of inducible *CreER*^{T} recombinase expression driven by the K8 upstream sequence. At 5-6 weeks of age, Tam was intraperitoneally administered to *K18-EG/K8CE*$^{tg/+}$*;R26R*$^{LacZ/+}$ bigenic and control (*R26R*$^{LacZ/+}$) mice, after which we examined inducible Cre activity by assessing X-gal staining, which reflected *LacZ* expression at 10 days after Tam treatment. We found that similar *LacZ* expression patterns were observed among the B, G, and H lines on the *R26R*$^{LacZ/+}$ background.

2.1 Evaluation of inducible Cre activity of *K18-EG/K8-CE*$^{tg/+}$*; R26R*$^{LacZ/+}$ bigenic mice across multiple organs

In the lower respiratory tract of bigenic mice, EGFP- and X-gal-positive staining was clearly observed in the trachea, bronchi, and bronchioles, but not in the alveoli (Fig 2BB′ and CC′). Histological sections of X-gal-stained tissues revealed that inducible Cre activity was mainly restricted in the pseudostratified epithelial cells of the terminal bronchiole (TB) (Fig 2C′) that expressed K8, which colocalized with EGFP fluorescence driven by the K18 upstream sequence (Fig 1B′), but Cre activity was not observed in the pneumocyte lining of the alveolar sac (AS) (Fig 2B and C). In the liver of bigenic mice, intense EGFP- and X-gal-positive staining revealed the organization of bile ducts or gross portal tracts (Fig 2D and E). Intense EGFP- and X-gal-positive staining was also visualized in the gallbladder (GB, Fig 2D and E). Through histological analysis and immunofluorescence staining using an antibody against K8, we found that intense K8 and EGFP expression was detected in the intrahepatic bile duct (BD) compared with that in the surrounding hepatocytes (Fig 2D′). Intensely X-gal-stained cells were mainly observed in the epithelial lining of the intrahepatic BD (Fig 2E′) and gallbladder (data not shown). Furthermore, bright EGFP-positive and intense X-gal-positive signals could be easily visualized in the pancreas, but not in the adjacent spleen (Fig 2F and G), of bigenic mice. Microscopically, pancreatic ducts (PDs) and exocrine acini expressed EGFP and K8 (Fig 2F′), which colocalized with X-gal staining (Fig 2G′).

Along the gastrointestinal tract of bigenic mice, the hind-stomach and intestine also exhibited bright EGFP fluorescence (Fig 2H and J) and the intense blue X-gal staining indicative of LacZ expression (Fig 2I and K). Immunostaining using an antibody against K8, together with EGFP fluorescence, revealed that both K8 and EGFP expression appeared in the epithelial cells of the hind stomach (Fig 2H′) and small intestine (Fig 2J′). Tam-induced LacZ expression was detected in the lower portion of zymogenic and parietal cells in the glandular hind stomach (Fig 2I′) and in crypts of the small intestine (Fig 2K′).

We further examined EGFP and induced LacZ expression in the reproductive tracts of bigenic mice (Fig 3). In the male reproductive tract, the seminal vesicles (SVs; Fig 3A and B) and epididymis (Fig 3E and F) exhibited intense EGFP expression and X-gal staining, whereas the testis exhibited neither LacZ nor EGFP expression (Fig 3E and F). In the prostate, the ventral prostate (VP) lobes and dorsolateral prostate (DLP) lobes exhibited strong LacZ and EGFP expression (Fig 3C and D) compared to that in the anterior prostate (AP) lobes (Fig 2A and B). Immunostaining of K8 was colocalized with EGFP fluorescence in the epithelial lining of the SV (Fig 3A′), the VP (Fig 3C′) and epididymis (Fig 3E′). In addition, the histological sections revealed X-gal-positive staining in the epithelia of corresponding organs (Fig 3B′, D′, and F′). Notably, patchy EGFP and X-gal signals partly overlapped with K8-expressing luminal cells of the AP (Fig 3A″ and B′′), indicative of inefficient expression of EGFP and LacZ in the AP of bigenic mice.

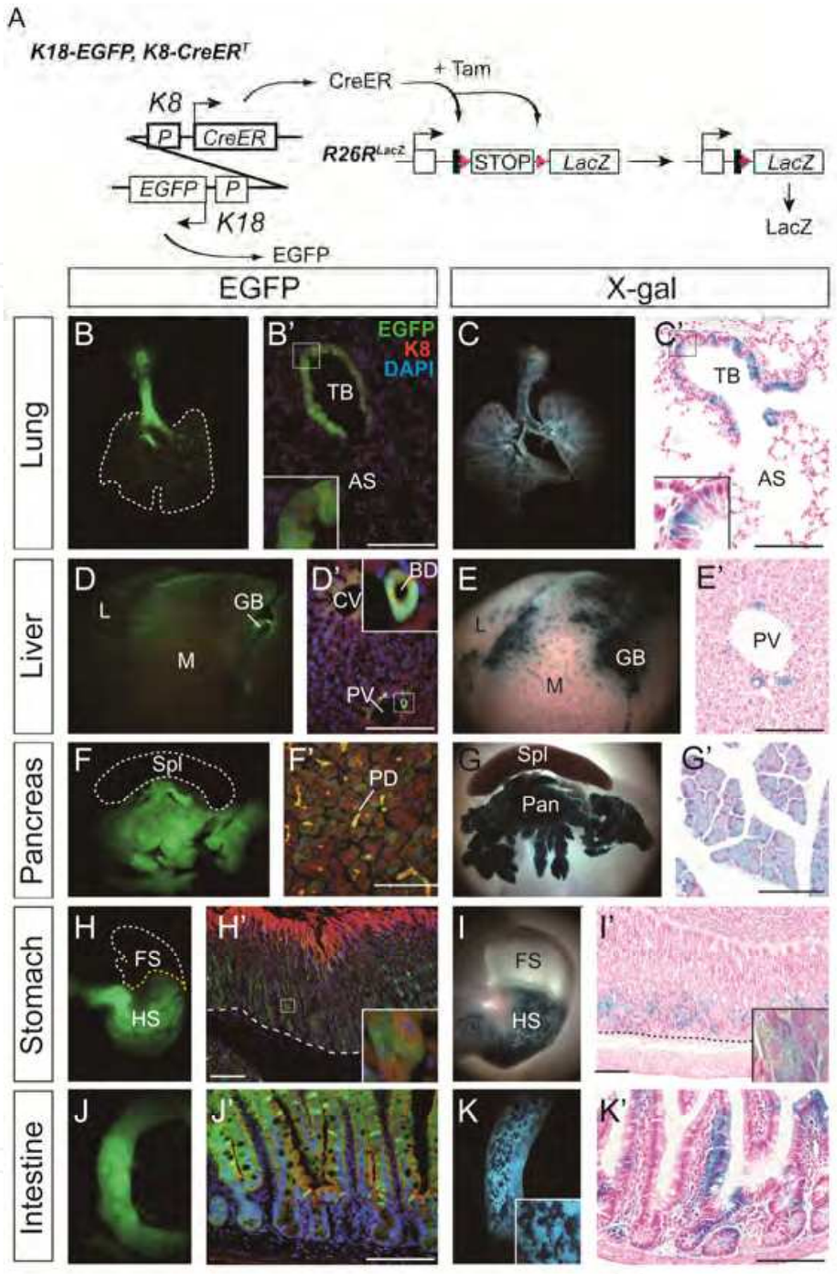

Fig. 2. Evaluation of the visualization marker EGFP and inducible Cre activity of *Tg(K18-EGFP, K8-CreER^T)* mice. (A) Schematic illustration of the genetic tool, *Tg(K18-EGFP, K8-CreER^T)* referred to *K18-EG/K8-CE*, which exhibits EGFP expression under the control of the K18 promoter and inducible Cre activity driven by the K8 promoter, which was evaluated by the Cre reporter allele, *R26R^{lacZ}*, after tamoxifen (Tam) administration. (B-K) Visualization of EGFP and evaluation of Tam-induced Cre-loxP recombination activity in the dissected organs of *K18-EG/K8-CE$^{tg/+}$;R26R$^{LacZ/+}$* mice treated with Tam for 10 days. (B) Whole-mount EGFP expression was visualized in the trachea, bronchus, and bronchiole of the *K18-EG/K8-CE$^{tg/+}$;R26R$^{LacZ/+}$* lung. (B') EGFP and immunofluorescent staining of K8 (red) revealed the colocalization of EGFP and K8 in the bronchiole columnar epithelium but not

in the AS. DAPI staining was used to indicate the nuclei. (C) The presence of LacZ expression was indicated by X-gal-stained epithelial tissues that had similar staining profiles as the EGFP-expressing tissue of the *K18-EG/K8-CE*$^{tg/+}$*;R26R*$^{LacZ/+}$ lung in (B). (C′) A histological section of the X-gal-stained lung was counterstained with Nuclear Fast Red to detect X-gal-stained epithelial cells. Insets in (B′) and (C′), high magnification of the epithelium of the terminal bronchiole (TB); (D) Intense EGFP expression was visualized as branching portal tracts in the *K18-EG/K8CE*$^{tg/+}$*;R26R*$^{LacZ/+}$ liver. GB, gallbladder; L, left liver lobe; M, medial liver lobe; (D′) EGFP and K8 expression was strongly detected in bile ducts (BDs) residing close to the portal vein (PV) and weakly detected in hepatocytes. CV, central vein; (E) Intense X-gal-positive blue patterns were similar to the EGFP expression patterns in the GB and branching portal tracts, but only patchy staining was observed in the liver parenchyma. (E′) Sections of whole-mount X-gal-stained liver exhibited strong blue staining in the BD. (F) and (G) Intense EGFP expression and the presence of LacZ were detected in the pancreas but not in the spleen (Spl). (F′) EGFP and K8 expression as positively detected in the exocrine acini and pancreatic ducts (PDs). (G′) Homogenous blue staining was histologically observed in the pancreatic acini and PDs. (H) and (I) Intense EGFP- and X-gal-positive staining was observed in the hind-stomach (HS), but not in the forestomach (FS). (H′) and (I′) EGFP and LacZ expression were highly localized at the base of the glandular stomach. (J) and (J′) Epithelial cells of the small intestine (jejunum) exhibited a strong EGFP signal. (K) and (K′) Mosaic LacZ activity revealed by X-gal staining in the crypts and upper differentiated epithelium of the jejunum. Scale bar, 100 μm.

In the reproductive tract of our bigenic females, EGFP was detected in the K8-expressing simple epithelium of the oviduct and uterus (Fig 3GG′ and II′). However, mosaic X-gal-positive patterns were observed in the simple epithelium of the oviduct and uterine glands (Fig 3 H′ and J′). Unexpectedly, LacZ and EGFP expression was not detected either grossly (Fig 3 G and H) or microscopically (Fig 3G′ and H′) in the ovarian surface epithelium (OSE; data not shown), which was thought to be the K8/K18-expressing cell type. The lack of EGFP and inducible LacZ expression in the OSE of bigenic mice indicated that the cis-regulatory elements within the K8-K18 intergenic sequence are unable to drive EGFP and CreER^{T} expression in the OSE.

2.2 Temporally controlled fate mapping to evaluate epithelial turnover in the mammary luminal epithelium and intestinal epithelium

In the adult stage, epithelial cell turnover is required to ensure the long-term maintenance of epithelial tissue homeostasis, which may be dysregulated during tumorigenesis. The process for epithelial renewal through generating new cells, differentiation, and migration from their stem/progenitors and niche varies among different epithelial tissues (Blanpain, Horsley and Fuchs 2007). As our *K18-EG/K8-CE*$^{tg/+}$*;R26R*$^{LacZ/+}$ mice were administered Tam by intraperitoneal injection at 6 weeks of age, we could monitor LacZ expression in various epithelial organs at different time points to determine whether inducible Cre activity occurred in higher hierarchical K8-expressing stem/progenitors to continuously give rise to their descendants. If the inducible Cre activity occurred in the stem/progenitors, then permanent LacZ activity could be detected in their descendants during cell turnover. In contrast, if the Tam-induced LacZ-expressing cells are terminally differentiated cells, then the LacZ-positive cells may be replaced by newly generated cells in which the *lox*P-flanked stop cassette of the *R26R* allele is not excised, indicating that these cells arise from K8-independent epithelial progenitors.

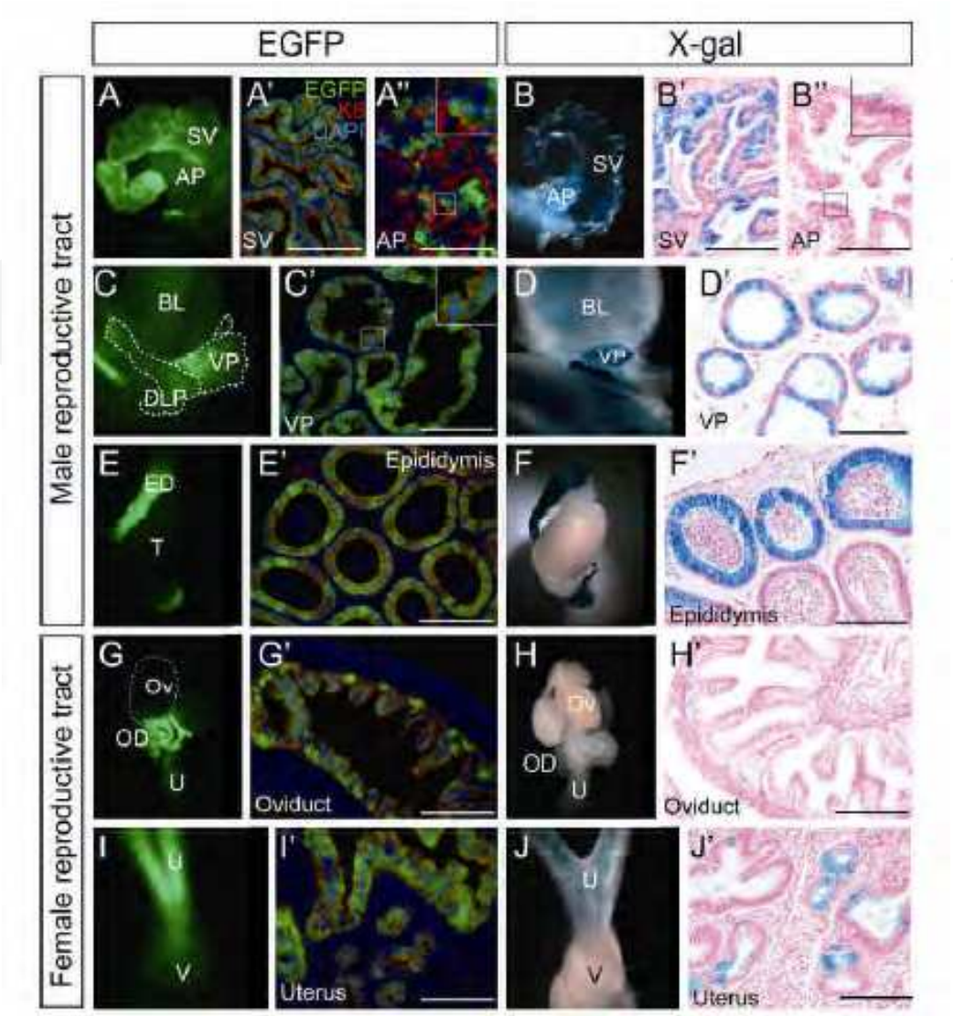

Fig. 3. EGFP visualization and evaluation of Tam-induced Cre activity in the reproductive organs of *K18-EG/K8-CE*$^{tg/+}$*;R26R*$^{LacZ/+}$ mice treated with Tam for 10 days. (A) and (B) The seminal vesicle (SV) exhibits greater EGFP and LacZ expression than the anterior prostate (AP). (A′) and (B′) Histological sections revealed an intensive EGFP signal (green) coexpressed with K8- (red) and X-gal-stained LacZ-expressing epithelia. (A′′) and (B′′) Histological sections revealed a weak mosaic EGFP signal (green) coexpressed with K8 (red) and few X-gal-stained cells, indicative of poor inducible Cre activity in the AP. (C) and (D) Whole-mount EGFP and LacZ were present in the bladder and prostate [ventral prostate (VP) and dorsolateral prostate (DLP)]. (C′) and (D′) Sections revealed intense EGFP and K8 coexpressing cells and X-gal-stained epithelia in the VP. (E) and (F) Intense EGFP- and X-gal-positive staining was clearly detected in the epididymis but not in the testis. (E′) and (F′) Histological sections of the epididymis exhibited an intense EGFP signal (green) coexpressed with K8 and LacZ activity. (G-J) In the female reproductive tract, an intense EGFP signal was observed in the oviduct (OD) and uterus (U), whereas X-gal staining was more strongly detected in the uterus. (G′-J′) Sections exhibited EGFP and K8 coexpression in the epithelia of the oviduct (G′) and uterus (I′), whereas mosaic X-gal-stained epithelia were observed in the corresponding organs (H′) and (J′). Scale bar, 100 μm.

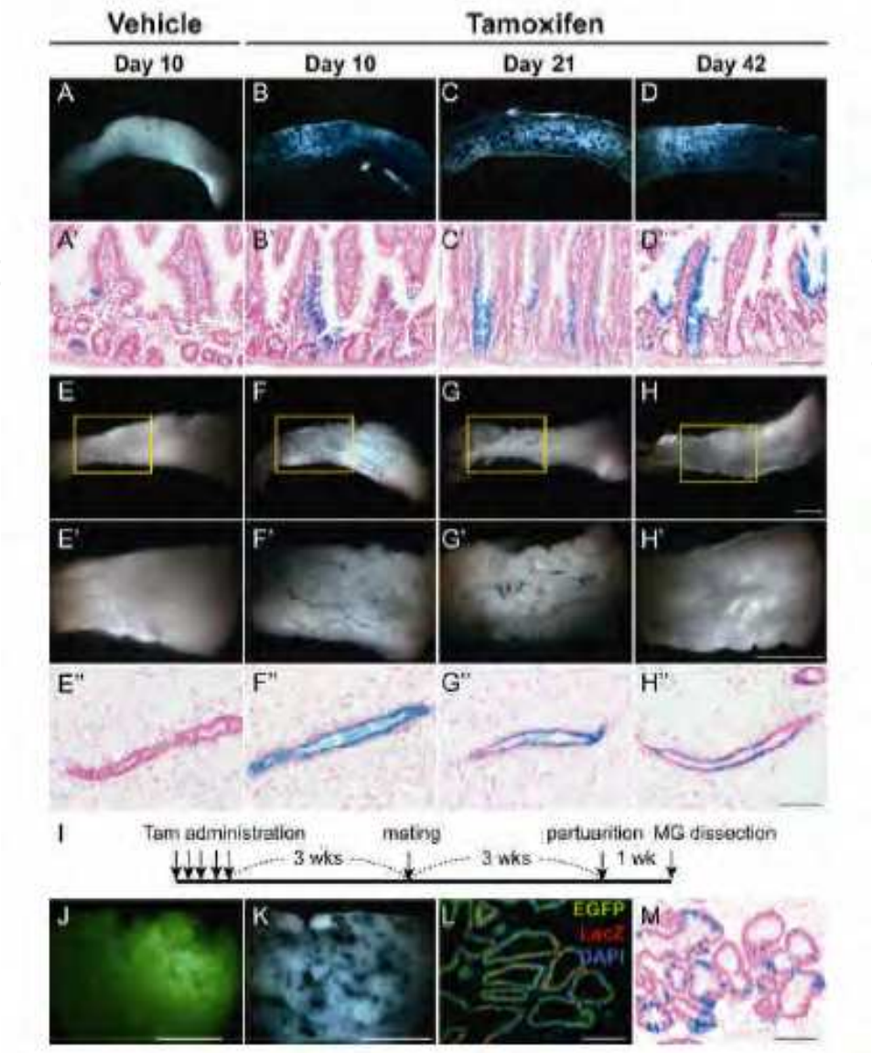

Fig. 4. Intestinal and mammary epithelial turnover monitored by LacZ activity in *K18-EG/K8-CE$^{tg/+}$;R26R$^{LacZ/+}$* mice. (A) Partial X-gal staining was detected in the intestines (jejunum) of the B line-derived *K18-EG/K8-CE$^{tg/+}$;R26R$^{LacZ/+}$* mice in the absence of Tam administration (vehicle treatment) after 10 days. (B-D) After Tam administration for 10, 21, and 42 days, intense X-gal staining patterns were clearly detected in the *K18-EG/K8-CE$^{tg/+}$;R26R$^{LacZ/+}$* intestines. (A'-D') Histological sections of the aforementioned samples were counterstained with Nuclear Fast Red, and they exhibited continuous X-gal-stained epithelial cells that emerged from the lower crypts to the upper absorptive cells in the *K18-EG/K8-CE$^{tg/+}$;R26R$^{LacZ/+}$* mice treated with Tam (B'-D') for 10-42 days. Conversely, a few X-gal-positive cells were detected in the intestines of vehicle-treated mice, indicating the leaky expression of LacZ. (E-H) Lower and (E'-H') higher magnification of X-gal-stained fourth mammary fat pads revealed the presence of X-gal-stained branching ducts in *K18-EG/K8-CE$^{tg/+}$;R26R$^{LacZ/+}$* mammary glands after Tam treatment for 10, 21, and 42 days (FF'-HH'), whereas no X-gal-stained cells were detected in the absence of Tam (EE'). (E''-H'') Histological sections of the aforementioned mammary samples were counterstained with Nuclear Fast Red, and they exhibited X-gal-stained luminal epithelia (F''-H'') in a time-

dependent manner in comparison to the staining in the vehicle control. (I) Timeline for the lineage tracing of a lactating mammary gland. The *K18-EG/K8-CE*$^{tg/+}$*;R26R*$^{LacZ/+}$ female was treated with Tam at 6 weeks of age and followed for 3 weeks to set up mating, and then the animal was analyzed at 1 week postparturition. (J-M) The dissected *K18-EG/K8-CE*$^{tg/+}$*;R26R*$^{LacZ/+}$ mammary gland was visualized by EGFP expression (J-L) and LacZ activity (K-M) both grossly and histologically. (L) Lactating alveolar epithelia of mammary glands exhibited uniform EGFP expression and mosaic patchy LacZ expression. Nuclei were counterstained with DAPI. (M) Histology sections were counterstained with Nuclear Fast Red, and they exhibited a mosaic pattern of X-gal-stained epithelial cells in the lactating mammary gland. Scale bars of A-D, E-H, and E′-H′, 0.25 cm; Scale bars of E′′-H′′ and L-M, 100 μm.

Complete epithelial turnover in the intestine requires approximately 5 days [for review, see (van der Flier and Clevers 2009)]. Conversely, the relatively slower turnover rate of mammary epithelial cells is regulated by the estrous cycle, and these cells undergo alveolar morphogenesis during pregnancy and lactation. Thus, we selectively monitored inducible LacZ activity in intestinal and mammary epithelia at 10, 21, and 42 days after Tam administration. In the absence of Tam administration (vehicle control), spotty X-gal signals were detected in the small intestine (Fig 4AA′), which indicated a leakage of inducible CreER^{T} activity, resulting in rare but detectable levels of LacZ expression. After 10 days of Tam administration, X-gal-stained intestinal epithelia were detected in the cell lineage that emerged from the crypts, differentiated, and migrated upward to the villi (Fig 4BB′). This phenomenon was also observed after 21 and 42 days of induction (Fig 4CC′ and DD′), indicating that the K8-expressing epithelia are composed of stem/progenitor cells that have the capability for long-term intestinal maintenance. In contrast, the numbers of X-gal-stained ductal cells in mammary glands gradually reduced after Tam treatment for 21 and 42 days (Fig 4G-G′′and H-H′′) compared to the number of X-gal-stained cells after 10 days of Tam treatment (Fig 4F). This observation suggests that the Tam-induced LacZ-expressing cells are replaced by newly generated cells from K8-independent epithelial origins, which give rise to LacZ-negative luminal cells that subsequently replace previous LacZ-positive cells to maintain mammary gland homeostasis.

3. Characterization of *Pten*-deficient epithelial tumors

3.1 The tumor latency, tumor spectrum, and tumor incidence of *K18-EG/K8-CE*$^{tg/+}$*; Pten*$^{fx/fx}$ mice

Throughout intensive analyses of inducible Cre activity controlled by the K8 promoter in various epithelial tissues as shown in Section 2, we further monitored epithelial tumors arising from *Pten*-deficient epithelial tissues to clarify the susceptibility of different epithelia to *Pten* loss in multiple organs. Thus, we generated *K18-EG/K8-CE*$^{tg/+}$*;Pten*$^{fx/+}$, *K18-EG/K8-CE*$^{tg/+}$*;Pten*$^{fx/fx}$ (referred to *K8-Pten*$^{fx/+}$ and *K8-Pten*$^{fx/fx}$, respectively), and their littermate controls and induced Cre-*lox*P recombination using Tam to excise exon 5 of *Pten* as illustrated in Fig 5A. All mice were on a mixed B6/129/Balb/c background.

Our results revealed that 92% of *K8-Pten*$^{fx/fx}$ mice (23/25) and 26.3% of *K8-Pten*$^{fx/+}$ mice (5/19) developed various malignant tumors by 60 and 100 weeks after Tam treatment, respectively (Fig 5B). The cumulative cancer-free survival is presented in Fig 5B. The overall mean latency of *Pten*-deficient tumors was approximately 25 weeks. All tumors were primarily analyzed by gross appearance and H&E-stained histology. The malignant tumors that developed in *K8-Pten*$^{fx/fx}$ and *K8-Pten*$^{fx/+}$ mice are summarized in Table 1.

We found that pancreatic ductal cancer (PDAC; 10 mice), cholangiocarcinoma (CC; 4 mice), hepatocellular carcinoma (HCC; 3 mice), and mammary gland tumors (MGTs; 7 females) accounted for the majority of the identified *Pten*-deficient malignancies (Fig 5C; Table 1), which are selectively described in Sections 3.2-3.4. Prostate cancer (two males) and precancerous lesions (prostate intraepithelial neoplasia) were also frequently found in *K8-Pten*$^{fx/fx}$ mice (data not shown). Other malignancies arising from the thyroid, lung, stomach, and uterus were occasionally identified in the *K8-Pten*$^{fx/fx}$ mice (Table 1). In addition, multiple tumors arising from different organs were observed in *K8-Pten*$^{fx/fx}$ mice (eight mice, 32%; three males and five females; Table 1). Moreover, five different epithelial malignancies arising from the thyroid, lung, pancreas, intestine, and breast were found in five *K8-Pten*$^{fx/+}$ females. At present, no malignant tumors have been found in *K8-Pten*$^{fx/+}$ males, which may be due to the limited animal numbers (n=7); a higher number of *K8-Pten*$^{fx/+}$ males might be required for further confirmation.

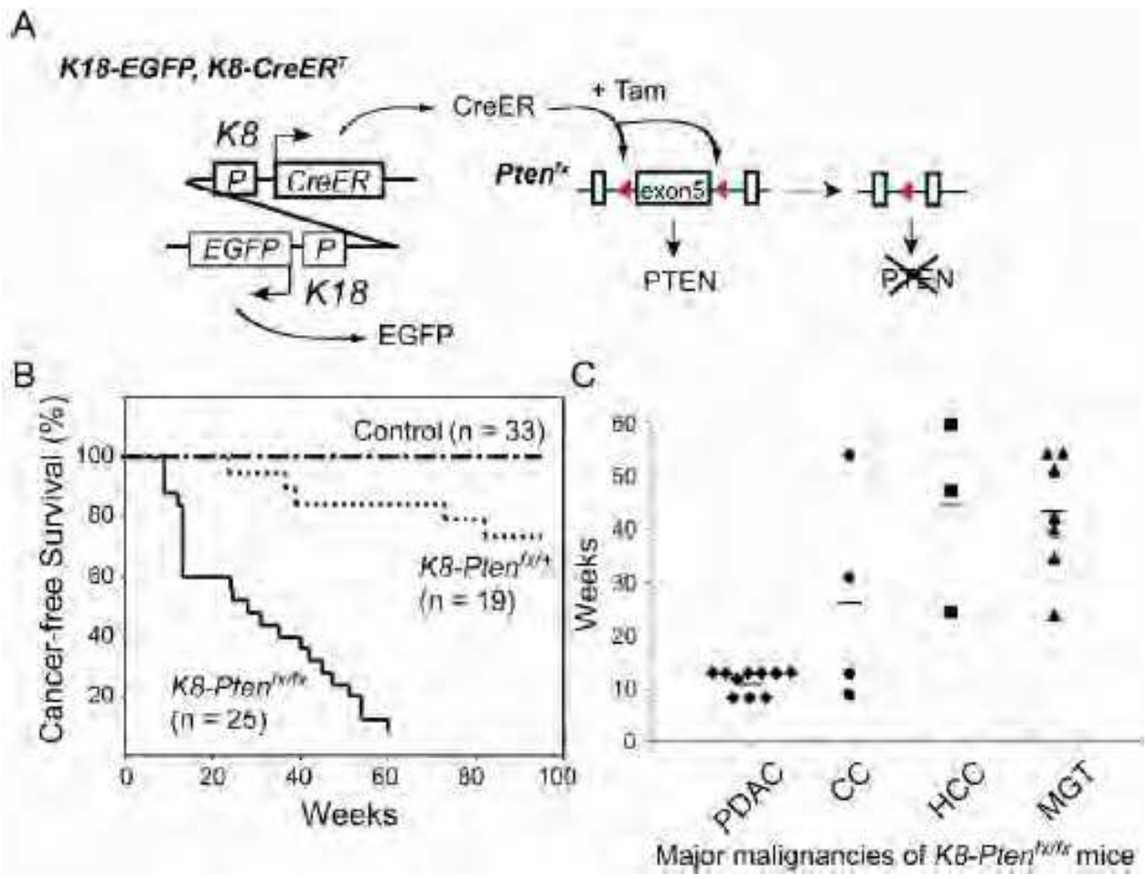

Fig. 5. Analysis of malignant tumors in the *K8-Pten*$^{fx/fx}$ and *K8-Pten*$^{fx/+}$ mice. (A) Schematic illustration of the genetic tool, *Tg(K18-EGFP, K8-CreER*^{T}*)*, used to conditionally excise the *Pten* floxed allele after Tam administration. (B) Cancer-free survival of control, *K8-Pten*$^{fx/+}$, and *K8-Pten*$^{fx/fx}$ mice. (C) Major epithelial malignancies (n≥3) of *K8-Pten*$^{fx/fx}$ mice. PDAC, pancreatic ductal cancer; CC, cholangiocarcinoma; HCC, hepatocellular carcinoma; MGT, mammary gland tumor.

	K8-Pten$^{fx/+}$	*K8-Pten*$^{fx/fx}$
Total animal number	19	25
male	7	7
female	12	18
Tumor incidence (%)	5 (26.3)	23 (92.0)
Tumor spectrum (%)		
Follicular thyroid carcinoma	1 (20.0)	1 (3.2)
Lung carcinoma	1 (20.0)	1 (3.2)
Pancreatic ductal adenocarcinoma	1 (20.0)	10 (32.3)
Intra-hepatic cholangiocarcinoma	0	4 (12.9)
Hepatocellular carcinoma	0	3 (9.7)
Gastrointestinal carcinoma	1 (20.0)	2 (6.5)
Prostate carcinoma	0	2 (6.5)
Endometrial carcinoma	0	1 (3.2)
Mammary gland tumor	1 (20.0)	7 (22.6)
Total tumor number	5	31*

*multiple tumors in 3 males and 5 females

Table 1. Malignancies of the *K8-Pten*$^{fx/+}$ and *K8-Pten*$^{fx/fx}$ mice.

3.2 *Pten*-deficient pancreatic malignancies

Among different tumor types, pancreatic malignancies developed approximately 12 weeks before other epithelial lesions, and pancreatic malignancies accounted for the majority of epithelial malignancies in Tam-treated *K8-Pten*$^{fx/fx}$ mice (Fig 5C). Pancreata isolated from control mice (Fig. 6 A-C) and sick *K8-Pten*$^{fx/fx}$ mice (Fig. 6 D-F, G-I, and J-L) were subjected to stereomicroscopy and histology. Grossly, the normal pancreas exhibited vasculature and a white appearance and was a soft organ connected to the caudal lobe of the liver, common bile duct, stomach, duodenum, and spleen (Fig. 6A). In the *Pten*-deficient pancreata, desmoplastic changes and cystic dilation could be identified (Fig. 6 D, G, and J). In addition, the higher EGFP intensity exhibited tubular or patchy patterns in the *K8-Pten*$^{fx/fx}$ mutants (Fig. 6 E, H, and K; arrows) compared to the uniform GFP pattern of the control (Fig. 6B). Microscopically, interlobular ductal hyperplasia (Fig. 6F), acinar-to-ductal metaplasia (Fig. 6I), and PDAC (Fig. 6L) were identified in some *K8-Pten*$^{fx/f}$ mice. In our observations, PDAC progression in *K8-Pten*$^{fx/fx}$ mice is an immediate life-threatening disease as like in humans. In general, our findings were consistent with an earlier report that characterized pancreatic ductal metaplasia and pancreatic cancer initiation in mice in which *Pten* was ablated by *Pdx1-Cre* starting from the developing pancreas specifically (Stanger et al. 2005). Our inducible Cre activity in the K8-expressing cells of the adult mouse pancreas likely includes pancreatic ducts and centroacinal cells in which *Pten* is excised, leading to PDAC.

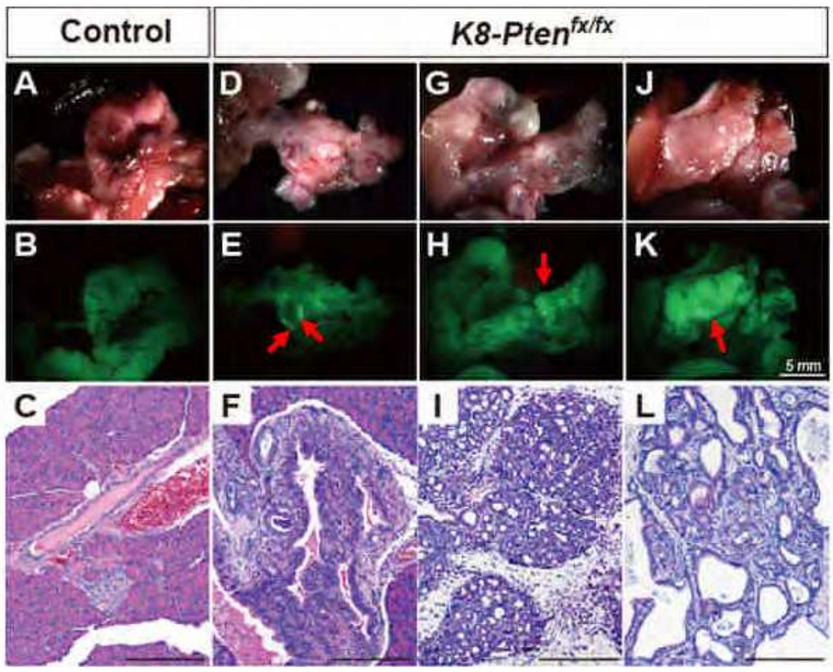

Fig. 6. Pancreatic malignancy of the *K8-Pten*$^{fx/fx}$ mice. Age-matched *Tg(K18-EGFP, K8-CreER)* pancreata were used as the control. Gross appearances and EGFP expression in control (A-B) and *K8-Pten*$^{fx/fx}$ pancreata (D-E, G-H, and J-K) were observed by stereomicroscopy. H&E-stained histological sections of control pancreata revealed the exocrine acinar gland, pancreatic islet, interlobular duct, and blood vessel (C). Interlobular ductal hyperplasia (F), ductal metaplasia (I), and invasive pancreatic ductal adenocarcinoma (L) were histologically identified in the *K8-Pten*$^{fx/fx}$ mice at 9-13 weeks after Tam treatment. Scale bar, 100 μm.

3.3 *Pten*-deficient MGTs

Previously, Li et al used a mammary-specific MMTV-Cre transgenic line to excise the *lox*P-floxed *Pten* critical exon (exon 5) (Li et al. 2002). Some *MMTV-Cre;Pten*$^{fx/fx}$ females develop MGTs as early as 2 months of age (Li et al. 2002). In our study, MGT was the most frequent (approximately 38.9%) malignancy in *K8-Pten*$^{fx/fx}$ females (7/18 mice). Palpable MGTs were detected at 24-54 weeks (mean latency, 43 weeks) after Tam treatment (Fig 5C), and they were dissected and observed under a stereomicroscope. We found that EGFP-positive branches were clearly revealed in the control mammary gland, although the deeper mammary branches were shielded by thick adipose tissue (Fig 7A). In the *K8-Pten*$^{fx/fx}$ mammary solid tumor, higher EGFP intensity was detected in a patchy pattern, which might represent a mass of hyperplastic epithelial cells (Fig 7B). Histologically, the representative *Pten*-deficient MGT was a solid epithelial mass with atypical glandular arrangement (Fig 7D) compared to the normal mammary ducts that were surrounded by adipose tissue (Fig 7C). To determine the effect of induced PTEN loss, we performed immunohistochemistry on the sections of the control and *K8-Pten*$^{fx/fx}$ mammary tissues. Our results revealed that PTEN expression could be detected in various cells, including ductal luminal and basal epithelial cells, vascular endothelial cells, and stromal cells, within the control mammary gland (Fig 7E). In contrast, the loss of PTEN was specifically demonstrated in the epithelial tumor cells, but not in the neovascular endothelial cells and stromal cells, of *K8-Pten*$^{fx/fx}$ MGTs (Fig 7F).

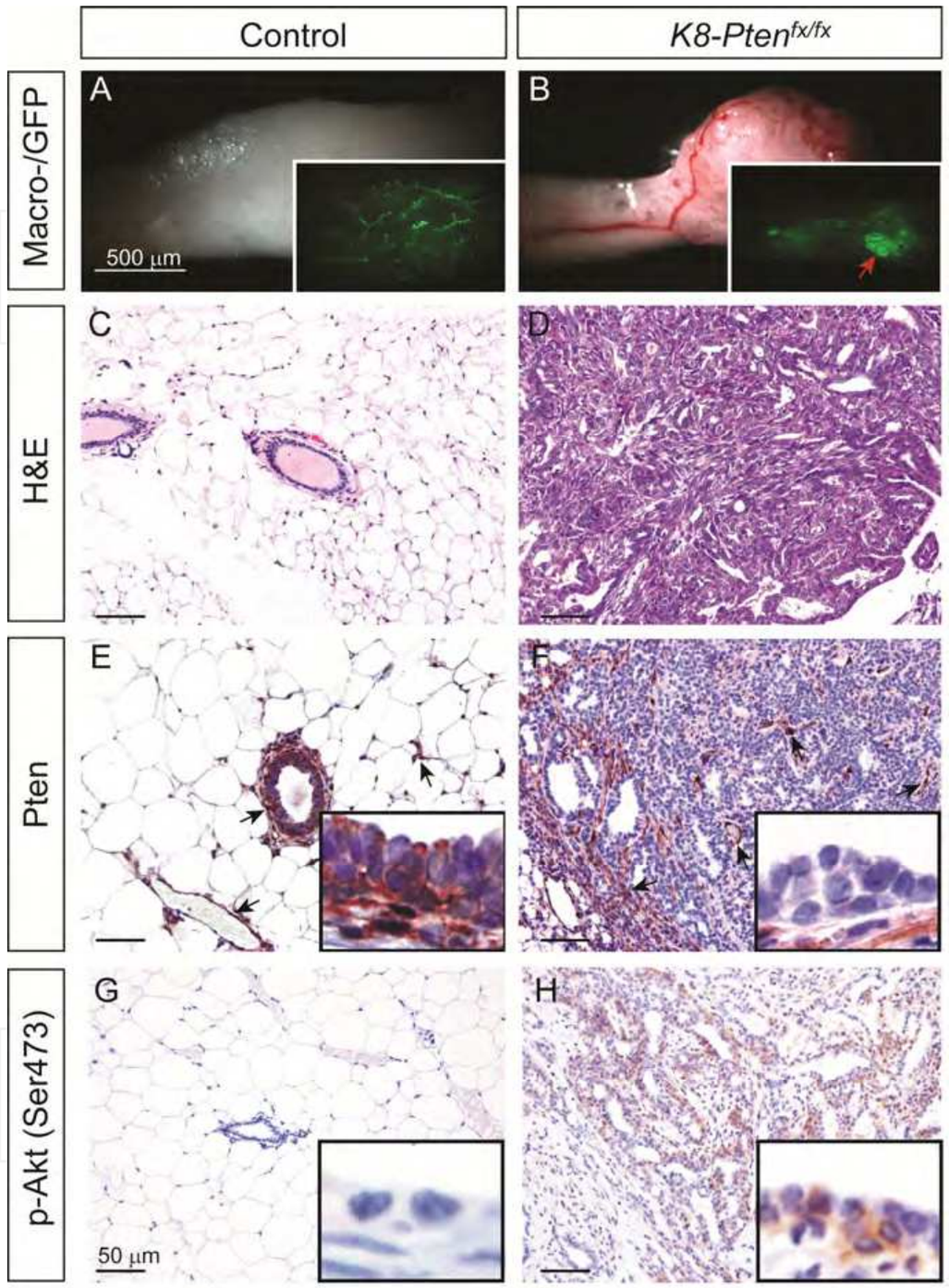

Fig. 7. Mammary tumors of the *K8-Pten*$^{fx/fx}$ females. (A) Mammary fat pad with EGFP-expressing ductal branches (inset) was obtained from a control female (42 weeks after Tam treatment); (B) MGT consisting of an EGFP-expressing tumor mass (inset) was obtained from a *K8-Pten*$^{fx/fx}$ female (42 weeks after Tam treatment); (C) and (D) H&E-stained histological sections of control mammary tissue (C; 54 weeks after Tam treatment) and *K8-Pten*$^{fx/fx}$ MGT (D; 54 weeks after Tam treatment); (E) and (F) PTEN immunohistochemistry

revealed the induced loss of PTEN in a *K8-Pten*$^{fx/fx}$ mammary epithelial tumor (F; 54 weeks after Tam treatment), whereas PTEN was expressed in various cell types within age-matched control mammary tissue (arrows; E). Insets, high-power views of the PTEN levels in the control mammary duct (E) and mammary epithelial tumor (F); (G) and (H) Immunohistochemistry of p-Akt(Ser473) revealed cytoplasmic staining of p-Akt in tubular structures infiltrating within a stroma of a *K8-Pten*$^{fx/fx}$ MGT (H; 35 weeks after Tam treatment) compared to a negatively stained mammary duct of an age-matched control mouse. Insets, high-power views of the p-Akt(Ser473) levels in the control mammary duct (G) and MGT (H). Scale bar (C-H), 100 µm.

Then, we determined activation of AKT using antibody against phosphorylated AKT, p-Akt(Ser473), and found that AKT phosphorylation appeared in the neoplastic epithelial cells of the *K8-Pten*$^{fx/fx}$ MGT (Fig 7H), unlike the controls (Fig 7G).Thus, our data revealed that the mammary luminal epithelium was highly susceptible to *Pten*-deficient mammary tumorigenesis, although it might be replaced by a K8^{+}-independent cell lineage as indicated by Cre reporter (LacZ) activity (Fig. 4E-H).

3.4 *Pten*-deficient HCCs and intrahepatic CCs

Liver-specific *Pten* ablation by albumin (Alb)-Cre has been reported to result in the development of steatohepatitis, metabolic disorders, and HCCs (Horie et al. 2004, Stiles et al. 2004). According to two different reports, the latency of *Pten*-deficient hepatocellular carcinogenesis appears to be required for an extended time. Horie et al reported that *Pten*-deficient HCCs developed in 66% of *Alb-Cre;Pten*$^{fx/fx}$ animals at 74-78 weeks of age. Xu et al also found that the incidence of HCCs was 33% by 12-16 months of age (Xu et al. 2006). Interestingly, Xu et al reported that their *Alb-Cre;Pten*$^{fx/fx}$ mice developed visible foci of CCs along with HCCs at late onset that were explained by the *Alb-Cre* mice exhibiting Cre activity in both hepatocytes and cholangiocytes (Xu et al. 2006). Moreover, early disease progression and higher penetrance of CCs were demonstrated when the Smad4 conditional allele was introduced into the *Alb-Cre;Pten*$^{fx/fx}$ background (Xu et al. 2006).

In our findings, low incidences of HCCs (3/25 mice) and CCs (4/25 mice) were identified in the Tam-treated *K8-Pten*$^{fx/fx}$ mice at 9-54 (mean latency, 27 weeks) and 24-60 weeks (mean latency, 44 weeks), respectively (Fig 5C). Our observations indicated a longer period of disease progression for HCCs than for CCs after *Pten* loss was induced. However, the relative susceptibilities of hepatocytes and cholangiocytes to *Pten*-deficient tumorigenesis remain unclear because of the low incidence of both diseases. Moreover, the induced mosaic Cre recombination events in the hepatocytes compared to the uniform and intense reporter (LacZ) activity in the cholangiocytes of bile ducts as shown in Fig 2E should also be considered because differential induction of Cre activity may directly contribute to the differential pace of disease progression initiated in hepatocytes compared to that initiated in cholangiocytes. Nevertheless, we could identify both fatty accumulation in hepatocytes (Fig 8A) and dysplastic/hyperplastic cholangiocytes of the dilated bile ducts (Fig 8B) in the sections of *K8-Pten*$^{fx/fx}$ livers at early time points (13 weeks) after Tam treatment. These early events might directly or indirectly lead to HCC (Fig 8D) and CC, which could be identified by K19 expression (Fig 8F), in the Tam-treated *K8-Pten*$^{fx/fx}$ mice at late onset.

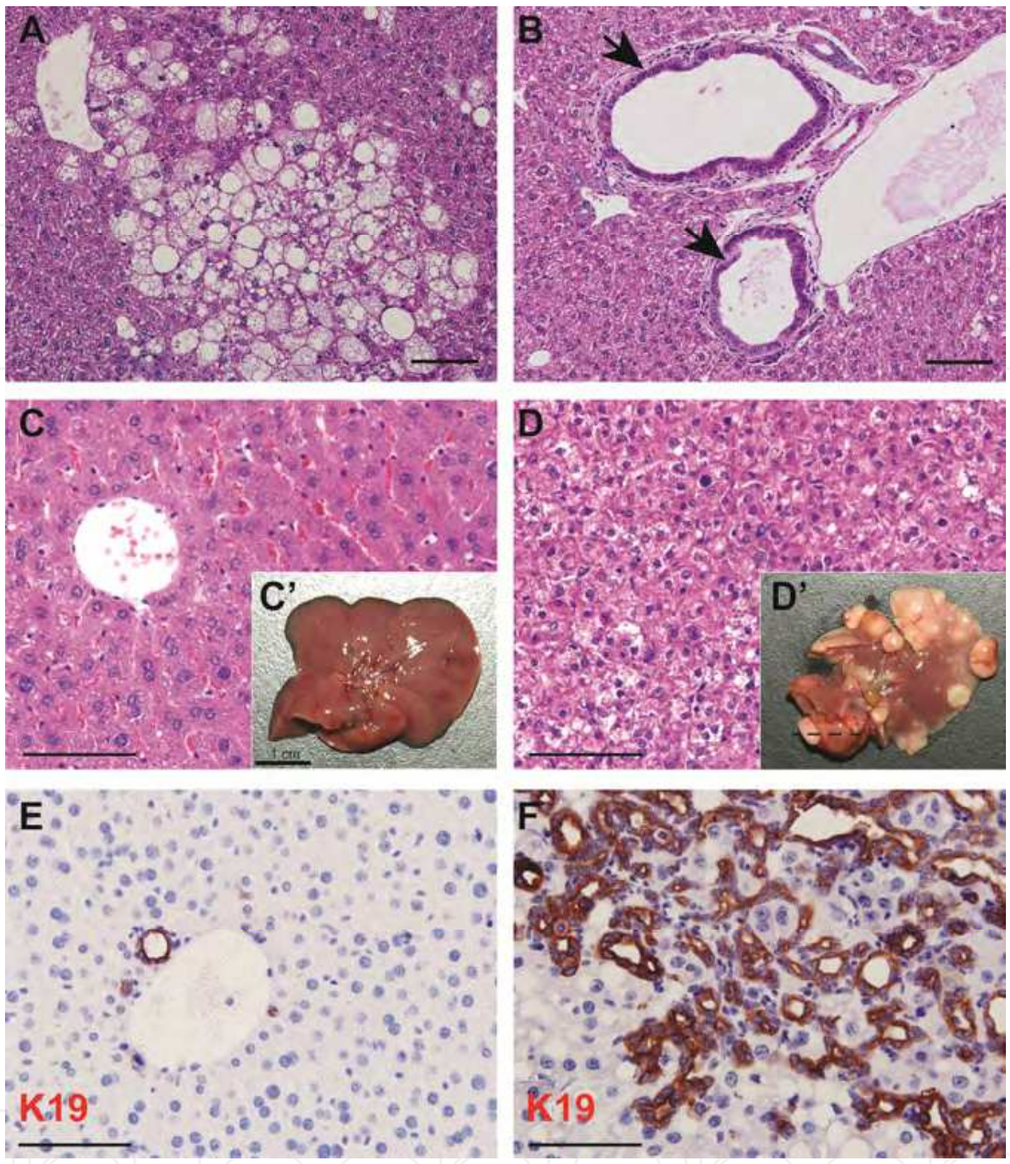

Fig. 8. Liver diseases of the *K8-Pten*$^{fx/fx}$ mice. (A) Fatty changes of hepatocytes in a *K8-Pten*$^{fx/fx}$ mouse at 13 weeks after Tam treatment; (B) Aberrant dilated bile ducts (arrows) of the portal tract in a *K8-Pten*$^{fx/fx}$ mouse at 13 weeks after Tam treatment; (C) H&E-stained section and gross view (C', inset) of a control liver at 60 weeks after Tam treatment; (D) H&E-stained section and gross view (D', inset) of a *K8-Pten*$^{fx/fx}$ liver at 60 weeks after Tam treatment; (E) and (F) K19 expressed in the control bile ductal cells (E) and in the acinar pattern of a representative *K8-Pten*$^{fx/fx}$ CC (31 weeks). Scale bar, 100 μm.

4. Conclusion

In this chapter, we demonstrated that the mouse *K8-K18* intergenic sequence possesses the essential promoters and regulatory elements for controlling the bidirectional expression of *CreER*^{T} and EGFP across multiple organs. Selectively ablating the tumor suppressor gene

Pten in the epithelial cells of multiple organs in this study provides an entry point to understand epithelial tissue susceptibility to *Pten*-deficient tumorigenesis. Our data reveal that the K8-expressing epithelia of the pancreatic ducts, prostate, and mammary glands are highly susceptible to *Pten*-deficient tumorigenesis. Hepatocytes and cholangiocytes of the liver also possibly undergo tumorigenesis after *Pten* loss, which may evoke a variety of downstream signaling circuits. All *Pten*-deficient malignancies described here are primary tumors that invade locally. Metastasis is rare in our current observation that requires further characterization. In the future, the same approach can possibly be used to establish clinically relevant mouse models to investigate adenocarcinoma initiation and progression by simultaneously creating additional genetic lesions in conjunction with the *K8-Pten*$^{fx/+}$ or *K8-Pten*$^{fx/fx}$ alleles; mice that carry multiple conditional alleles of cancer-related genes can be generated and characterized to understand tumor susceptibility, considering that cancer is a disease of multiple genetic events.

5. Acknowledgment

We thank Yi-Hsuan Chiang, Yu-Lei Chang, Ming-Lun Lee and Wan-Chun Yu for their initial assistance. Authors also thank all members of the laboratories of C.-M. C. (cmchen@ym.edu.tw) and of L.-R. Y. (lryou@ym.edu.tw) for helpful discussion. This work was supported by a grant from the National Health Research Institutes (NHRI-EX99-9901-BI), a grant from the Ministry of Education "Aim for the Top University Plan", grants from the National Science Council (NSC 98-2320-B010-011-MY3, NSC 99-3112-B010-013 (99IR017) to C.M.C. and a technical service was supported by the Taiwan Mouse Clinic (NSC 99-3112-B-001-021).

Note: Methods used in this chapter were described previously (Chen and Behringer 2004, Chen, Chang and Behringer 2004, Chen et al. 2010, Liang et al. 2009, Lu et al. 2007).

6. References

Alessi, D. R., S. R. James, C. P. Downes, A. B. Holmes, P. R. Gaffney, C. B. Reese & P. Cohen (1997) Characterization of a 3-phosphoinositide-dependent protein kinase which phosphorylates and activates protein kinase Balpha. *Curr Biol,* 7**,** 261-9.

Ali, I. U., L. M. Schriml & M. Dean (1999) Mutational spectra of PTEN/MMAC1 gene: a tumor suppressor with lipid phosphatase activity. *J Natl Cancer Inst,* 91**,** 1922-32.

Blanpain, C., V. Horsley & E. Fuchs (2007) Epithelial stem cells: turning over new leaves. *Cell,* 128**,** 445-58.

Brown, E. J., P. A. Beal, C. T. Keith, J. Chen, T. Bum Shin & S. L. Schreiber (1995) Control of p70 S6 kinase by kinase activity of FRAP in vivo. *Nature,* 377**,** 441-446.

Brunet, A., A. Bonni, M. J. Zigmond, M. Z. Lin, P. Juo, L. S. Hu, M. J. Anderson, K. C. Arden, J. Blenis & M. E. Greenberg (1999) Akt Promotes Cell Survival by Phosphorylating and Inhibiting a Forkhead Transcription Factor. *Cell,* 96**,** 857-868.

Brunn, G. J., C. C. Hudson, A. Sekuli, J. M. Williams, H. Hosoi, P. J. Houghton, J. C. Lawrence, Jr. & R. T. Abraham. 1997. Phosphorylation of the Translational Repressor PHAS-I by the Mammalian Target of Rapamycin. 99-101.

Carracedo, A. & P. P. Pandolfi (2008) The PTEN-PI3K pathway: of feedbacks and cross-talks. *Oncogene,* 27**,** 5527-41.

Chen, C. M. & R. R. Behringer (2004) Ovca1 regulates cell proliferation, embryonic development, and tumorigenesis. *Genes Dev,* 18**,** 320-32.

Chen, C. M., J. L. Chang & R. R. Behringer (2004) Tumor formation in p53 mutant ovaries transplanted into wild-type female hosts. *Oncogene,* 23**,** 7722-5.

Chen, C. M., H. Y. Wang, L. R. You, R. L. Shang & F. C. Liu (2010) Expression analysis of an evolutionary conserved metallophosphodiesterase gene, Mpped1, in the normal and beta-catenin-deficient malformed dorsal telencephalon. *Dev Dyn,* 239**,** 1797-806.

Cross, D. A., D. R. Alessi, P. Cohen, M. Andjelkovich & B. A. Hemmings (1995) Inhibition of glycogen synthase kinase-3 by insulin mediated by protein kinase B. *Nature,* 378**,** 785-9.

Cully, M., H. You, A. J. Levine & T. W. Mak (2006) Beyond PTEN mutations: the PI3K pathway as an integrator of multiple inputs during tumorigenesis. *Nat Rev Cancer,* 6**,** 184-92.

Datta, S. R., H. Dudek, X. Tao, S. Masters, H. Fu, Y. Gotoh & M. E. Greenberg (1997) Akt Phosphorylation of BAD Couples Survival Signals to the Cell-Intrinsic Death Machinery. *Cell,* 91**,** 231-241.

Dunlop, E. A. & A. R. Tee (2009) Mammalian target of rapamycin complex 1: Signalling inputs, substrates and feedback mechanisms. *Cellular Signalling,* In Press, Corrected Proof.

Fang, D., D. Hawke, Y. Zheng, Y. Xia, J. Meisenhelder, H. Nika, G. B. Mills, R. Kobayashi, T. Hunter & Z. Lu. 2007. Phosphorylation of beta-Catenin by AKT Promotes beta-Catenin Transcriptional Activity. 11221-11229.

Fujita, N., S. Sato, K. Katayama & T. Tsuruo (2002) Akt-dependent phosphorylation of p27Kip1 promotes binding to 14-3-3 and cytoplasmic localization. *J Biol Chem,* 277**,** 28706-13.

Hara, K., K. Yonezawa, M. T. Kozlowski, T. Sugimoto, K. Andrabi, Q.-P. Weng, M. Kasuga, I. Nishimoto & J. Avruch. 1997. Regulation of eIF-4E BP1 Phosphorylation by mTOR. 26457-26463.

He, X. C., T. Yin, J. C. Grindley, Q. Tian, T. Sato, W. A. Tao, R. Dirisina, K. S. Porter-Westpfahl, M. Hembree, T. Johnson, L. M. Wiedemann, T. A. Barrett, L. Hood, H. Wu & L. Li (2007) PTEN-deficient intestinal stem cells initiate intestinal polyposis. *Nat Genet,* 39**,** 189-98.

Horie, Y., A. Suzuki, E. Kataoka, T. Sasaki, K. Hamada, J. Sasaki, K. Mizuno, G. Hasegawa, H. Kishimoto, M. Iizuka, M. Naito, K. Enomoto, S. Watanabe, T. W. Mak & T. Nakano (2004) Hepatocyte-specific Pten deficiency results in steatohepatitis and hepatocellular carcinomas. *J Clin Invest,* 113**,** 1774-83.

Inoki, K., Y. Li, T. Zhu, J. Wu & K.-L. Guan (2002) TSC2 is phosphorylated and inhibited by Akt and suppresses mTOR signalling. *Nat Cell Biol,* 4**,** 648-657.

Kishimoto, H., K. Hamada, M. Saunders, S. Backman, T. Sasaki, T. Nakano, T. W. Mak & A. Suzuki (2003) Physiological functions of Pten in mouse tissues. *Cell Struct Funct,* 28**,** 11-21.

Lesche, R., M. Groszer, J. Gao, Y. Wang, A. Messing, H. Sun, X. Liu & H. Wu (2002) Cre/loxP-mediated inactivation of the murine Pten tumor suppressor gene. *Genesis,* 32**,** 148-9.

Li, D. M. & H. Sun (1997) TEP1, encoded by a candidate tumor suppressor locus, is a novel protein tyrosine phosphatase regulated by transforming growth factor beta. *Cancer Res,* 57**,** 2124-9.

Li, G., G. W. Robinson, R. Lesche, H. Martinez-Diaz, Z. Jiang, N. Rozengurt, K. U. Wagner, D. C. Wu, T. F. Lane, X. Liu, L. Hennighausen & H. Wu (2002) Conditional loss of PTEN leads to precocious development and neoplasia in the mammary gland. *Development,* 129**,** 4159-70.

Li, J., C. Yen, D. Liaw, K. Podsypanina, S. Bose, S. I. Wang, J. Puc, C. Miliaresis, L. Rodgers, R. McCombie, S. H. Bigner, B. C. Giovanella, M. Ittmann, B. Tycko, H. Hibshoosh, M. H. Wigler & R. Parsons (1997) PTEN, a putative protein tyrosine phosphatase gene mutated in human brain, breast, and prostate cancer. *Science,* 275**,** 1943-7.

Liang, C.-C., L. R. You, J.-L. Chang, T.-F. Tsai & C.-M. Chen (2009) Transgenic mice exhibiting inducible and spontaneous Cre activities driven by a bovine keratin 5 promoter that can be used for the conditional analysis of basal epithelial cells in multiple organs. *J Biomed. Sci.,* 16**,** 2.

Lu, T.-L., J.-L. Chang, C.-C. Liang, L.-R. You & C.-M. Chen (2007) Tumor Spectrum, Tumor Latency and Tumor Incidence of the Pten-Deficient Mice. *PLoS ONE,* 2**,** e1237.

Manning, B. D. & L. C. Cantley (2007) AKT/PKB signaling: navigating downstream. *Cell,* 129**,** 1261-74.

Manning, B. D., A. R. Tee, M. N. Logsdon, J. Blenis & L. C. Cantley (2002) Identification of the Tuberous Sclerosis Complex-2 Tumor Suppressor Gene Product Tuberin as a Target of the Phosphoinositide 3-Kinase/Akt Pathway. *Molecular Cell,* 10**,** 151-162.

Mayo, L. D. & D. B. Donner (2001) A phosphatidylinositol 3-kinase/Akt pathway promotes translocation of Mdm2 from the cytoplasm to the nucleus. *Proc Natl Acad Sci U S A,* 98**,** 11598-603.

Peso, L. d., M. Gonzalez-Garcia, C. Page, R. Herrera & G. Nunez. 1997. Interleukin-3-Induced Phosphorylation of BAD Through the Protein Kinase Akt. 687-689.

Sarbassov, D. D., S. M. Ali, D. H. Kim, D. A. Guertin, R. R. Latek, H. Erdjument-Bromage, P. Tempst & D. M. Sabatini (2004) Rictor, a novel binding partner of mTOR, defines a rapamycin-insensitive and raptor-independent pathway that regulates the cytoskeleton. *Curr Biol,* 14**,** 1296-302.

Sarbassov, D. D., D. A. Guertin, S. M. Ali & D. M. Sabatini (2005) Phosphorylation and regulation of Akt/PKB by the rictor-mTOR complex. *Science,* 307**,** 1098-101.

Soriano, P. (1999) Generalized lacZ expression with the ROSA26 Cre reporter strain. *Nat Genet,* 21**,** 70-1.

Stambolic, V., A. Suzuki, J. L. de la Pompa, G. M. Brothers, C. Mirtsos, T. Sasaki, J. Ruland, J. M. Penninger, D. P. Siderovski & T. W. Mak (1998) Negative regulation of PKB/Akt-dependent cell survival by the tumor suppressor PTEN. *Cell,* 95**,** 29-39.

Stanger, B. Z., B. Stiles, G. Y. Lauwers, N. Bardeesy, M. Mendoza, Y. Wang, A. Greenwood, K. H. Cheng, M. McLaughlin, D. Brown, R. A. Depinho, H. Wu, D. A. Melton & Y. Dor (2005) Pten constrains centroacinar cell expansion and malignant transformation in the pancreas. *Cancer Cell,* 8**,** 185-95.

Steck, P. A., M. A. Pershouse, S. A. Jasser, W. K. Yung, H. Lin, A. H. Ligon, L. A. Langford, M. L. Baumgard, T. Hattier, T. Davis, C. Frye, R. Hu, B. Swedlund, D. H. Teng & S. V. Tavtigian (1997) Identification of a candidate tumour suppressor gene, MMAC1, at chromosome 10q23.3 that is mutated in multiple advanced cancers. *Nat Genet,* 15**,** 356-62.

Stiles, B., Y. Wang, A. Stahl, S. Bassilian, W. P. Lee, Y. J. Kim, R. Sherwin, S. Devaskar, R. Lesche, M. A. Magnuson & H. Wu (2004) Liver-specific deletion of negative regulator Pten results in fatty liver and insulin hypersensitivity [corrected]. *Proc Natl Acad Sci U S A,* 101**,** 2082-7.

van der Flier, L. G. & H. Clevers (2009) Stem cells, self-renewal, and differentiation in the intestinal epithelium. *Annu Rev Physiol,* 71**,** 241-60.

Wu, X., K. Senechal, M. S. Neshat, Y. E. Whang & C. L. Sawyers (1998) The PTEN/MMAC1 tumor suppressor phosphatase functions as a negative regulator of the phosphoinositide 3-kinase/Akt pathway. *Proc Natl Acad Sci U S A,* 95**,** 15587-91.

Xu, X., S. Kobayashi, W. Qiao, C. Li, C. Xiao, S. Radaeva, B. Stiles, R. H. Wang, N. Ohara, T. Yoshino, D. LeRoith, M. S. Torbenson, G. J. Gores, H. Wu, B. Gao & C. X. Deng (2006) Induction of intrahepatic cholangiocellular carcinoma by liver-specific disruption of Smad4 and Pten in mice. *J Clin Invest,* 116**,** 1843-52.

Zhou, B. P., Y. Liao, W. Xia, B. Spohn, M.-H. Lee & M.-C. Hung (2001a) Cytoplasmic localization of p21Cip1/WAF1 by Akt-induced phosphorylation in HER-2/neu-overexpressing cells. *Nat Cell Biol,* 3**,** 245-252.

Zhou, B. P., Y. Liao, W. Xia, Y. Zou, B. Spohn & M. C. Hung (2001b) HER-2/neu induces p53 ubiquitination via Akt-mediated MDM2 phosphorylation. *Nat Cell Biol,* 3**,** 973-82.

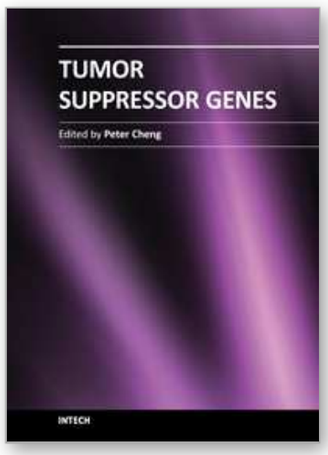

Tumor Suppressor Genes

Edited by Dr. Yue Cheng

ISBN 978-953-307-879-3
Hard cover, 332 pages
Publisher InTech
Published online 03, February, 2012
Published in print edition February, 2012

Functional evidence obtained from somatic cell fusion studies indicated that a group of genes from normal cells might replace or correct a defective function of cancer cells. Tumorigenesis that could be initiated by two mutations was established by the analysis of hereditary retinoblastoma, which led to the eventual cloning of RB1 gene. The two-hit hypothesis helped isolate many tumor suppressor genes (TSG) since then. More recently, the roles of haploinsufficiency, epigenetic control, and gene dosage effects in some TSGs, such as P53, P16 and PTEN, have been studied extensively. It is now widely recognized that deregulation of growth control is one of the major hallmarks of cancer biological capabilities, and TSGs play critical roles in many cellular activities through signaling transduction networks. This book is an excellent review of current understanding of TSGs, and indicates that the accumulated TSG knowledge has opened a new frontier for cancer therapies.

InTech Europe
University Campus STeP Ri
Slavka Krautzeka 83/A
51000 Rijeka, Croatia
Phone: +385 (51) 770 447
Fax: +385 (51) 686 166
www.intechopen.com

InTech China
Unit 405, Office Block, Hotel Equatorial Shanghai
No.65, Yan An Road (West), Shanghai, 200040, China
中国上海市延安西路65号上海国际贵都大饭店办公楼405单元
Phone: +86-21-62489820
Fax: +86-21-62489821

IntechOpen